IET Radar Sonar and Navigation, Volume 11, Issue 7, July 2017, pp. 1132-1139
DOI:10.1049/iet-rsn.2016.0547

Coordination of optimal guidance law and adaptive radiated waveform for interception and rendezvous problems

Alessio Balleri[1], Alfonso Farina[2] and Alessio Benavoli[3]

Abstract

We present an algorithm that allows an interceptor aircraft equipped with an airborne radar to meet another air target (the intercepted) by developing a guidance law and automatically adapting and optimising the transmitted waveform on a pulse to pulse basis. The algorithm uses a Kalman filter to predict the relative position and speed of the interceptor with respect to the target. The transmitted waveform is automatically selected based on its ambiguity function and accuracy properties along the approaching path. For each pulse, the interceptor predicts its position and velocity with respect to the target, takes a measurement of range and radial velocity and, with the Kalman filter, refines the relative range and range rate estimates. These are fed into a Linear Quadratic Gaussian (LQG) controller that ensures the interceptor reaches the target automatically and successfully with minimum error and with the minimum guidance energy consumption.

Index Terms

Rendezvous, interception, adaptive radar waveform, chirp, Ambiguity Function, Fisher Information Matrix, Cramér-Rao Lower Bound, narrowband, wideband, Linear Quadratic Gaussian control, Kalman Filter, predator-prey, bat echolocation waveform.

[1]A. Balleri, Centre for Electronic Warfare, Information and Cyber, Cranfield University, Defence Academy of the UK, Shrivenham, SN6 8LA, UK, e-mail: a.balleri@cranfield.ac.uk.

[2]A. Farina, FIET, LFIEEE, Selex-ES (retired), Visiting Professor UCL, Rome, Italy, e-mail: alfonso.farina@outlook.it

[3]A. Benavoli, Istituto ”Dalle Molle” di Studi sull’Intelligenza Artificiale (IDSIA), Galleria 2, CH-6928, Manno (Lugano), Switzerland, alessio@idsia.ch

I. List of symbols

$\mathbf{x_b}$, $\mathbf{x_f}$, $\mathbf{e}$	N_{x} x 1	State vectors of interceptor, target and error between the two state vectors
$\mathbf{w_b}$, $\mathbf{w_f}$, $\mathbf{w_e}$	N_w x 1	Noisy perturbation of interceptor, target and error dynamic state equations
$\mathbf{u}$	N_u x 1	Control input signal to the interceptor
$\mathbf{y_e}$	N_{y} x 1	Measurement of the error between state vectors
$\boldsymbol{\nu}_e$	N_{y} x 1	Additive noise for the measurement of the error
$\mathbf{P}_k$	N_{x} x N_{x}	Estimation error covariance matrix at time k
$\mathbf{P}_{k\|k-1}$	N_{x} x N_{x}	Prediction of the estimation error covariance matrix at time k
$\mathbf{Q}$	N_{x} x N_{x}	Covariance matrix of the forcing noise of the error state equation
$\mathbf{F}$	N_{x} x N_{x}	State transition matrix
$\mathbf{M}$	N_{x} x N_{x}	Cost function matrix
$\mathbf{U}_k$	N_{x} x N_{x}	Dynamic Riccati equation matrix at time k
$\mathbf{S}_k$	N_{y} x N_{y}	Residual covariance matrix at time k
$\mathbf{H}$	N_{y} x N_{x}	Measurement matrix
$\mathbf{K}_k$	N_{x} x N_{y}	Kalman gain at time k
$\mathbf{G}$	N_{x} x N_{w}	Process noise matrix
$\mathbf{R}$	N_{u} x N_{u}	Cost function matrix
$\mathbf{L}_k$	N_{u} x N_{x}	Feedback gain matrix at time k
$\mathbf{B}$	N_{x} x N_{u}	Control transition matrix

II. Introduction

The task of intercepting a target and/or rendezvous is an important technical challenge that occurs in many defence operations as well as in civilian applications like robotics, Simultaneous Localisation And Map (SLAM) and similar [1]. One of the first papers on optimal guidance for interception and rendezvous dates back to 1971 [2]. In that paper, a sensor on the ground delivers optimal guidance to the interceptor on the basis of the estimated trajectories of the interceptor and the target to reach. The radar transmits a suitable waveform which, however, does not change during the task. Another paper [3] years later develops a procedure to adapt the radiated waveform to minimise the estimation error in a tracking study case. This procedure has been recently named fore-active control. It is known [4] that a bat looking for a prey (e.g. a moth or a butterfly) during its search, acquisition, tracking and interception phases along its trajectory to approach the prey changes adaptively the radiated waveform of the calls in order to improve the location of the prey. More precisely, the figures from [5] [6] show the time-frequency spectrogram of the radiated calls in the successive phases of the interception. It can be argued that the bat develops an optimal rendezvous trajectory together with an adaptive radiated waveform which improves the location capability of the predator. Another interesting reference on the subject is [7].

In this paper we take inspiration from the bat and develop an algorithm that guides an airborne radar interceptor towards a target by jointly developing an optimal guidance and automatically adapting and optimising the transmitted waveform on a pulse to pulse basis. We suitably combine the techniques in [2] and [3], namely the optimal

linear quadratic Gaussian (LQG) control law and the fore-active control of the radiated waveform. This is an original contribution of the paper. The result which we achieve is to emulate what the bat does in its predation: contemporaneously and interactively develop an optimal approaching trajectory and transmit a waveform that adaptively changes during the approaching trajectory phases so that the measurements of the sensor on board of the interceptor are better suited to improve guidance law. Some preliminary results of the proposed technique were presented in [8].

III. Theoretical framework

We study the case of an interceptor and a target both moving with the same type of linear kinematics described by a matrix $\mathbf{F}$. The trajectory of both the interceptor and the target are subject to Gaussian random perturbations, $\mathbf{Gw_f}(k-1)$ and $\mathbf{Gw_b}(k-1)$, with zero mean value and covariance matrices $\mathbf{Q_f}$ and $\mathbf{Q_b}$, respectively.

$$\begin{aligned}\mathbf{x_f}(k) &= \mathbf{F}\mathbf{x_f}(k-1) + \mathbf{G}\mathbf{w_f}(k-1)\\ \mathbf{x_b}(k) &= \mathbf{F}\mathbf{x_b}(k-1) + \mathbf{B}\mathbf{u}(k-1) + \mathbf{G}\mathbf{w_b}(k-1)\end{aligned} \tag{1}$$

The term $\mathbf{Bu}(k-1)$ is used to model the ability of the interceptor to adapt and control its trajectory at each step. The interceptor is modelled as a controlled system that accepts an input vector $\mathbf{u}(k)$ which is combined linearly with a matrix $\mathbf{B}$ before being applied to the equations describing the target kinematics. We define the difference between the state equations of the interceptor and of the target as the error to reduce to the minimum value at the intercept point

$$\mathbf{e}(k) = \mathbf{x_b}(k) - \mathbf{x_f}(k) = \mathbf{F}\mathbf{e}(k-1) + \mathbf{B}\mathbf{u}(k-1) + \mathbf{G}\mathbf{w_e}(k-1) \tag{2}$$

with $\mathbf{Gw_e}(k-1)$ being a Gaussian random process with mean value zero and covariance matrix $\mathbf{Q}$. At each time k the interceptor transmits a waveform to measure its relative distance and radial velocity with respect to the target and uses the measurements to control its trajectory in order to intercept the target with a limited number of transmissions N_T and with the minimum energy consumption. We assume that the measurement $\mathbf{y_e}(k)$ of the distance and velocity relative to each transmission is a linear function of the error $\mathbf{e}(k)$ as [3]

$$\mathbf{y_e}(k) = \mathbf{H}\mathbf{e}(k) + \boldsymbol{\nu}_e(k;\boldsymbol{\theta}_k) \tag{3}$$

where $\mathbf{H}$ is the matrix that maps the error into the measurement and $\boldsymbol{\nu}_e(k;\boldsymbol{\theta}_k)$ is a Gaussian random process with mean value zero and a covariance matrix $\mathbf{N}(\boldsymbol{\theta}_k)$. The covariance matrix of each measurement depends on the accuracy of the transmitted waveform $s(t;\boldsymbol{\theta}_k)$ whose design is fully described by the vector of parameters $\boldsymbol{\theta}_k$ that identifies the key waveform properties, such as duration, bandwidth and time-frequency curvature. The mathematical expression of the elements of $\boldsymbol{\theta}_k$ and the vector length depend on the waveform design. It has been shown in the literature that $\mathbf{N}(\boldsymbol{\theta}_k)$ corresponds to the Cramér-Rao Lower Bound (CRLB), relative to the task of joint estimation of range and radial velocity between a sensor and a target, when the sensor transmits the signal $s(t;\boldsymbol{\theta}_k)$ [9] [10] [11] [12]. The Fisher Information Matrix (FIM) for range and radial velocity in the presence of noise with mean power N_0 can be expressed as

$$\text{FIM} = -\text{SNR} \left(\begin{array}{cc} \frac{4}{c^2}\frac{1}{2}\frac{\partial^2|\chi(\tau,\nu;\boldsymbol{\theta}_k)|^2}{\partial\tau^2} & \frac{4}{c\lambda}\frac{1}{2}\frac{\partial^2|\chi(\tau,\nu;\boldsymbol{\theta}_k)|^2}{\partial\tau\partial\nu} \\ \frac{4}{c\lambda}\frac{1}{2}\frac{\partial^2|\chi(\tau,\nu;\boldsymbol{\theta}_k)|^2}{\partial\nu\partial\tau} & \frac{4}{\lambda^2}\frac{1}{2}\frac{\partial^2|\chi(\tau,\nu;\boldsymbol{\theta}_k)|^2}{\partial\nu^2} \end{array} \right) \Bigg|_{\tau,\nu=0} \tag{4}$$

where c is the speed of propagation, λ is the wavelength , $\text{SNR} = 2E_s/N_0$ is the Signal to Noise Ratio and $\chi_k(\tau,\nu)$ is the normalised narrowband Complex Ambiguity Function (CAF) of the signal $\sqrt{E_s}s(t;\boldsymbol{\theta}_k)$ of energy E_s defined as

$$\chi(\tau,\nu;\boldsymbol{\theta}_k) = \int_{-\infty}^{\infty} s(t;\boldsymbol{\theta}_k)s^*(t+\tau;\boldsymbol{\theta}_k)e^{j2\pi\nu t}dt \tag{5}$$

The CRLB is obtained as the inverse of FIM and therefore

$$\mathbf{N}(\boldsymbol{\theta}_k) = [\text{FIM}]^{-1} \tag{6}$$

This gives the minimum values of variances and covariances of the measurements of range and range rate. At each time k, the interceptor makes a prediction of the estimation error covariance matrix

$$\mathbf{P}_{k|k-1} = \mathbf{F}\mathbf{P}_{k-1}\mathbf{F}^T + \mathbf{Q} \tag{7}$$

and then selects the waveform parameters $\boldsymbol{\theta}_k$ so to minimise the determinant of the residual matrix

$$\mathbf{S}_k = \mathbf{H}\mathbf{P}_{k|k-1}\mathbf{H}^T + \mathbf{N}(\boldsymbol{\theta}_k) \tag{8}$$

as described in [3]. The interceptor then produces a pulse, takes a measurement with a waveform of the preselected parameters $\boldsymbol{\theta}_k$, and uses the covariance matrix $\mathbf{N}(\boldsymbol{\theta}_k)$ to calculate the Kalman filter gain $\mathbf{K}_k$ as

$$\mathbf{K}_k = \mathbf{P}_{k|k-1}\mathbf{H}^T\mathbf{S}_k^{-1} \tag{9}$$

The Kalman gain is then used to calculate the estimation error covariance matrix at the kth step as $\mathbf{P}_k = (\mathbf{I} - \mathbf{K}_k\mathbf{H})\,\mathbf{P}_{k|k-1}$ and an estimate of the error as

$$\begin{aligned} \hat{\mathbf{e}}(k|k-1) &= \mathbf{F}\hat{\mathbf{e}}(k-1) + \mathbf{B}\mathbf{u}(k-1) \\ \hat{\mathbf{e}}(k) &= \hat{\mathbf{e}}(k|k-1) + \mathbf{K}_k\left[\mathbf{y}_\mathbf{e}(k) - \mathbf{H}\hat{\mathbf{e}}(k|k-1)\right] \end{aligned} \tag{10}$$

Eq. 10 shows that the estimate of the error at the kth time step only depends on the control input at the k-1th time and this will allow us to select the most appropriate control input at the kth time based solely on the estimate of the error.

As previously mentioned, the control task is carried out to ensure the interceptor reaches the target as efficiently as possible. To do this, we define and minimise the cost function

$$J = E\left\{\mathbf{e}^T(N_T)\mathbf{M}\mathbf{e}(N_T) + \sum_{k=0}^{N_T}\mathbf{u}^T(k)\mathbf{R}\mathbf{u}(k)\right\} \tag{11}$$

of the kind of a typical LQG control framework [2]. In Eq. 11, N_T is the predefined number of transmissions used to intercept the target and $\mathbf{M}$ and $\mathbf{R}$ are two suitable matrices that are applied to the dynamic state error and to the input control signal, respectively. It is worth noting that when $\mathbf{M}$ and $\mathbf{R}$ are identity matrices the cost function is

minimised when the error at time N_T is minimised and when the energy of the input signal $\mathbf{u}(k)$ is also minimised. The solution of Eq. 11 is well known in the literature (e.g. see [2]) and it is such that the control input signal at the time k is a function of the estimate of the error at the time k and of a matrix $\mathbf{L}_k$

$$\mathbf{u}(k) = -\mathbf{L}_k \hat{\mathbf{e}}(k) \tag{12}$$

where

$$\mathbf{L}_k = \left(\mathbf{B}^T \mathbf{U}_k \mathbf{B} + \mathbf{R}\right)^{-1} \mathbf{B}^T \mathbf{U}_k \mathbf{F} \tag{13}$$

and

$$\mathbf{U}_k = \mathbf{F}^T \left(\mathbf{U}_{k+1} - \mathbf{U}_{k+1}\mathbf{B}\left(\mathbf{B}^T \mathbf{U}_{k+1}\mathbf{B} + \mathbf{R}\right)^{-1} \mathbf{B}^T \mathbf{U}_{k+1}\right) \mathbf{F} \text{ , with } \mathbf{U}_{N_T} = \mathbf{M} \tag{14}$$

We note that the interleave between fore-active control and LQG control is new and represents one of the contributions of this paper.

A. Gaussian Linear Chirp

In this paper, we limit the study to Linear Frequency Modulated chirps (LFM) with a Gaussian amplitude modulation of the form

$$s(t;\boldsymbol{\theta}_k) = \left(\frac{1}{\pi\lambda_G^2}\right)^{\frac{1}{4}} e^{-\frac{t^2}{2\lambda_G^2}} e^{jb_G t^2} e^{j2\pi f_0 t} \tag{15}$$

whose design depends solely on the parameters λ_G and b_G, that is $\boldsymbol{\theta}_k = [b_G\ \lambda_G]^T$. Selecting and diversifying these parameters results in waveforms with a different time duration $T = 2\lambda_G$ and bandwidth $B = b_G T/\pi$. The use of a Gaussian linear chirp simplifies the analysis because the FIM relative to this class of waveforms is known in the literature (e.g see [3] and [13]) and can be expressed as

$$\text{FIM} = \text{SNR} \begin{pmatrix} \frac{4}{c^2}\left(\frac{1}{2\lambda_G^2} + 2\lambda_G^2 b_G^2\right) & \frac{4}{c\lambda}\left(2\pi\lambda_G^2 b_G\right) \\ \frac{4}{c\lambda}\left(2\pi\lambda_G^2 b_G\right) & \frac{4}{\lambda^2}\left(2\pi^2\lambda_G^2\right) \end{pmatrix} \tag{16}$$

which leads to

$$\mathbf{N}(\boldsymbol{\theta}_k) = \begin{pmatrix} \frac{c^2\lambda_G^2}{2\text{SNR}} & -\frac{c\lambda\lambda_G^2 b_G}{2\pi\text{SNR}} \\ -\frac{c\lambda\lambda_G^2 b_G}{2\pi\text{SNR}} & \frac{\lambda^2}{4\pi^2\text{SNR}}\left(\frac{1}{2\lambda_G^2} + 2\lambda_G^2 b_G^2\right) \end{pmatrix} \tag{17}$$

It can be easily shown that the determinant of the FIM is equal to $\text{SNR}^2 \frac{16\pi^2}{c^2\lambda^2}$ and does not depend on the parameters b_G and λ_G [3]. This will significantly simplify the calculations of the optimal $\boldsymbol{\theta}_k$ in the next section.

IV. Case Study

We study the case of an interceptor and a target that move along a mono-dimensional path. The state variables of both the interceptor and the target consist of the position, the velocity and the acceleration and a noisy perturbation is applied to the component representing the acceleration. We use the classical equations developed in [14] and used in [3], thus define the matrices $\mathbf{F}$ and $\mathbf{G}$ as

$$\mathbf{F} = \begin{pmatrix} 1 & T_s & \frac{T_s^2}{2} \\ 0 & 1 & T_s \\ 0 & 0 & 1 \end{pmatrix} \tag{18}$$

and

$$\mathbf{G} = \begin{pmatrix} 0 \\ 0 \\ 1 \end{pmatrix} \tag{19}$$

where T_s is the radar scan period [1]

The sensor measures the distance between the predator and the prey and their relative radial velocity. When both the predator and the prey move over a line the measurements corresponds to the measurement of the error $\mathbf{y_e}$ when the matrix $\mathbf{H}$ is defined as

$$\mathbf{H} = \begin{pmatrix} 1 & 0 & 0 \\ 0 & 1 & 0 \end{pmatrix} \tag{20}$$

For the mono-dimensional case and for the matrix $\mathbf{H}$ defined as above, the matrix $\mathbf{S}_k$ becomes equal to

$$\mathbf{S}_k = \begin{pmatrix} p_{11} + n_{11} & p_{12} + n_{12} \\ p_{12} + n_{12} & p_{22} + n_{22} \end{pmatrix} \tag{21}$$

where p_{ij} and n_{ij} are respectively the elements of the matrix $\mathbf{P}_{k|k-1}$ and $\mathbf{N}(\boldsymbol{\theta}_k)$, and its determinant can be expressed as

$$\det(\mathbf{S}_k) = \left[p_{1,1}p_{2,2} - p_{1,2}^2\right] + p_{1,1}n_{2,2} + +p_{2,2}n_{1,1} - 2p_{1,2}n_{1,2} + \det(\mathbf{N}(\boldsymbol{\theta}_k)) \tag{22}$$

The minimum of the determinant of $\mathbf{S}_k$ is obtained by deriving Eq. 22 with respect to λ_G and b_G after noting that the elements $p_{i,j}$ and the determinant of $\mathbf{N}(\boldsymbol{\theta}_k)$ do not depend on the waveform parameters. It has been demonstrated in [3] that, as a result of this minimisation, the waveform parameters of the Gaussian linear chirp $\boldsymbol{\theta}_k = \begin{bmatrix} b_G & \lambda_G \end{bmatrix}^T$ at the k-th time step can be simply calculated as

$$\begin{aligned} b_G &= -\frac{w_c p_{12}}{2p_{11}} \\ \lambda_G &= \left(\frac{p_{11}^2}{w_c^2(p_{11}p_{22} - p_{12}^2)}\right)^{1/4} \end{aligned} \tag{23}$$

The derivation of these equations is straightforward and results from the non-dependency of the determinant of the covariance matrix of the measurements on the parameters which is a key property of the Gaussian chirp [3].

A. Simulation results

Results are presented for the notional case of a radar interceptor required to meet a target within $N = 60$ scans with a scan period $T_s = 0.5$ ms. For simplicity, we have assumed that the radar transmits one pulse per scan at a central frequency $f_0 = 10$ GHz. At reception phase, a matched filter is applied followed by the conventional measurement parameters extraction. We have performed a Monte Carlo simulation of which we show the results for just one run. The initial values of the error state vector $\mathbf{e}(0)$ have been set so that the initial distance between the interceptor and the target is 10 km and the initial relative velocity and acceleration are -200 m/s and 0 m/s^2,

[1] In this paper we only consider the case of one pulse per scan and hence the scan period corresponds to the Pulse Repetition Interval (PRI) of the radar.

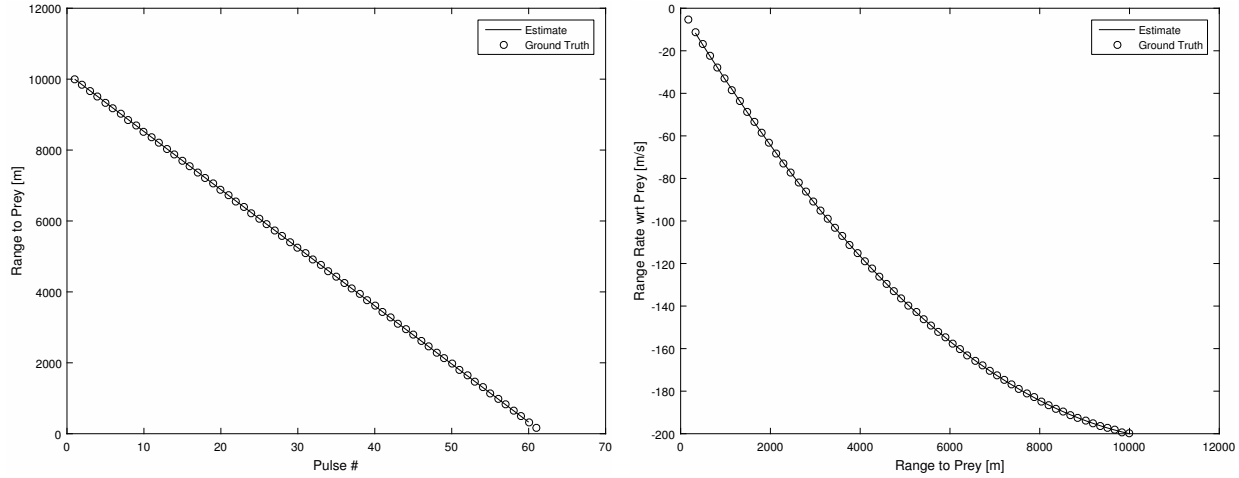

(a) Range vs Pulse

(b) Range vs Range-rate

Fig. 1. a) Distance between the interceptor and the target at each transmission and b) Plot of the estimated range and velocity with respect to the ground truth at each transmission. The plots are relative to one Monte Carlo realisation.

respectively. The relative position, velocity and acceleration are then varied throughout the mission by means of the LQG controller. The SNR at the beginning of the task is 15 dB. The covariance matrix $\mathbf{Q}$ of the error state vector is defined as $\mathbf{Q} = \mathbf{G}\sigma^2\mathbf{G}^T$ where σ^2 is the variance of the zero-mean Gaussian process that describes the relative acceleration between the interceptor and the target. The variance of the relative acceleration is set to $\sigma^2 = 0.1$ m^2/s^4 and

$$\mathbf{B} = \begin{pmatrix} 1 & 0 \\ 0 & 1 \\ 0 & 0 \end{pmatrix} \tag{24}$$

Results have been produced with a correct estimate of the error at time $k = 0$ (i.e. $\hat{\mathbf{e}}(0) = \mathbf{e}(0)$), with an estimation error covariance matrix $\mathbf{P}_0$ equal to identity and with $\mathbf{u}(0) = [0\,0]^T$. The LQG controller has been set with both the matrices $\mathbf{M}$ and $\mathbf{R}$ being equal to identity. The minimum possible pulse duration the algorithm can select at each time is constrained so to avoid eclipsing and is calculated as $T_{min}(k) = 2d(k)/c$, where $d(k)$ is the amplitude of the first element of $\hat{\mathbf{e}}(k)$. Similarly, the bandwidth is constrained at each step to meet the minimum range resolution requirements. In the simulations, the minimum bandwidth B_{min} is fixed to 5 MHz, corresponding to a range resolution of 30 m. The energy of the transmitted waveform is constant from pulse to pulse and the SNR increases at each step only for effect of the decrease in relative range between the interceptor and the target.

Figure 1 shows the plots of the relative distance between the interceptor and the target as a function of time and the range-velocity diagram for each pulse. Results clearly show that the LQG guidance law is such that the interceptor reaches the target successfully within the pre-established number of scans. The velocity profile shows that interceptor velocity is higher at the beginning of the attack and then diminishes as the interceptor approaches the target. Figure 2 shows the optimal duration and bandwidth of the Gaussian LFM that are automatically selected by the algorithm at each scan. Results show that the pulse duration decreases as the interceptor closes in and that

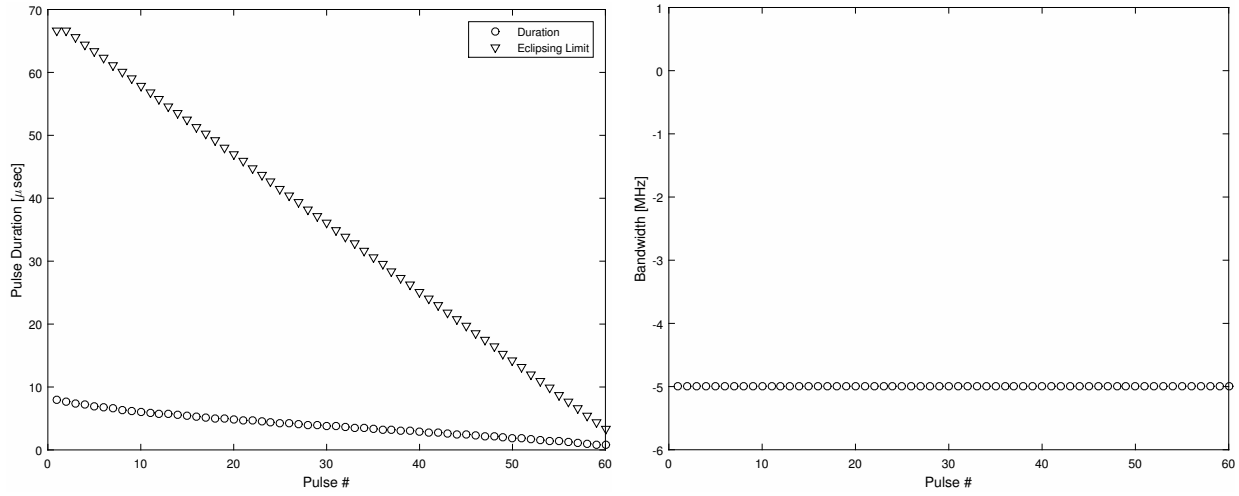

(a) Pulse Duration (b) Bandwidth

Fig. 2. a) Duration and b) bandwidth of the chirp with Gaussian envelope as a function of the transmitted pulse number. The plots are relative to one Monte Carlo realisation.

the bandwidth remains constant and equal to B_{min}. As a result, the compression factor of the matched filter to the received chirp also decreases. The optimal pulse duration is smaller than T_{min} at each scan, indicating that the constraint on the minimum allowable pulse duration, set to avoid eclipsing, does not have an impact on the automatic selection. Decreasing the pulse duration along the trajectory has the effect of improving the time-delay measurement accuracy when the interceptor becomes closer to the target (see element (1,1) of the matrix $\mathbf{N}(\boldsymbol{\theta}_k)$ in Eq. 17). Figure 3 shows the AF of the 1$^{\text{st}}$, 15$^{\text{th}}$, 45$^{\text{th}}$ and 60$^{\text{th}}$ transmitted waveforms. Results show that the wedge of the AF rotates anti-clockwise along the trajectory. When the interceptor approaches the target, the bandwidth does not change significantly and the range resolution remains constant. However, as the pulse duration becomes shorter the Doppler resolution decreases. The waveform is Doppler tolerant throughout the mission[2], that is the output of the matched-filter remains high in the presence of a Doppler mismatch. Figure 4 shows the plots of the rotating AF superimposed to the range-velocity diagram.

Figure 5 shows the Short Time Fourier Transform (STFT) of the same pulses of Figure 3. Results show that, as expected, because the bandwidth is the same throughout the mission and the pulse duration shortens, the time-frequency slope becomes steeper in the proximity of the target. This results is in agreement with the case of a bat intercepting its prey. The bat, in fact, also shortens the duration of the echolocation calls, whilst spanning a large bandwidth, in the terminal phase of a typical feeding buzz [4] [6].

The results presented above are relative to the case when a constraint on the bandwidth of the transmitted waveform was applied to meet a range resolution requirement. For completeness, Figure 6 and Figure 7 show the results for the case when the algorithm was left free to select any values of the parameter b_G at each step. Figure 6 shows that the interceptor successfully reaches the target within the pre-defined number of transmissions as expected. The

[2]Doppler tolerance is a characteristic of linear chirps when the narrowband approximation is satisfied [13].

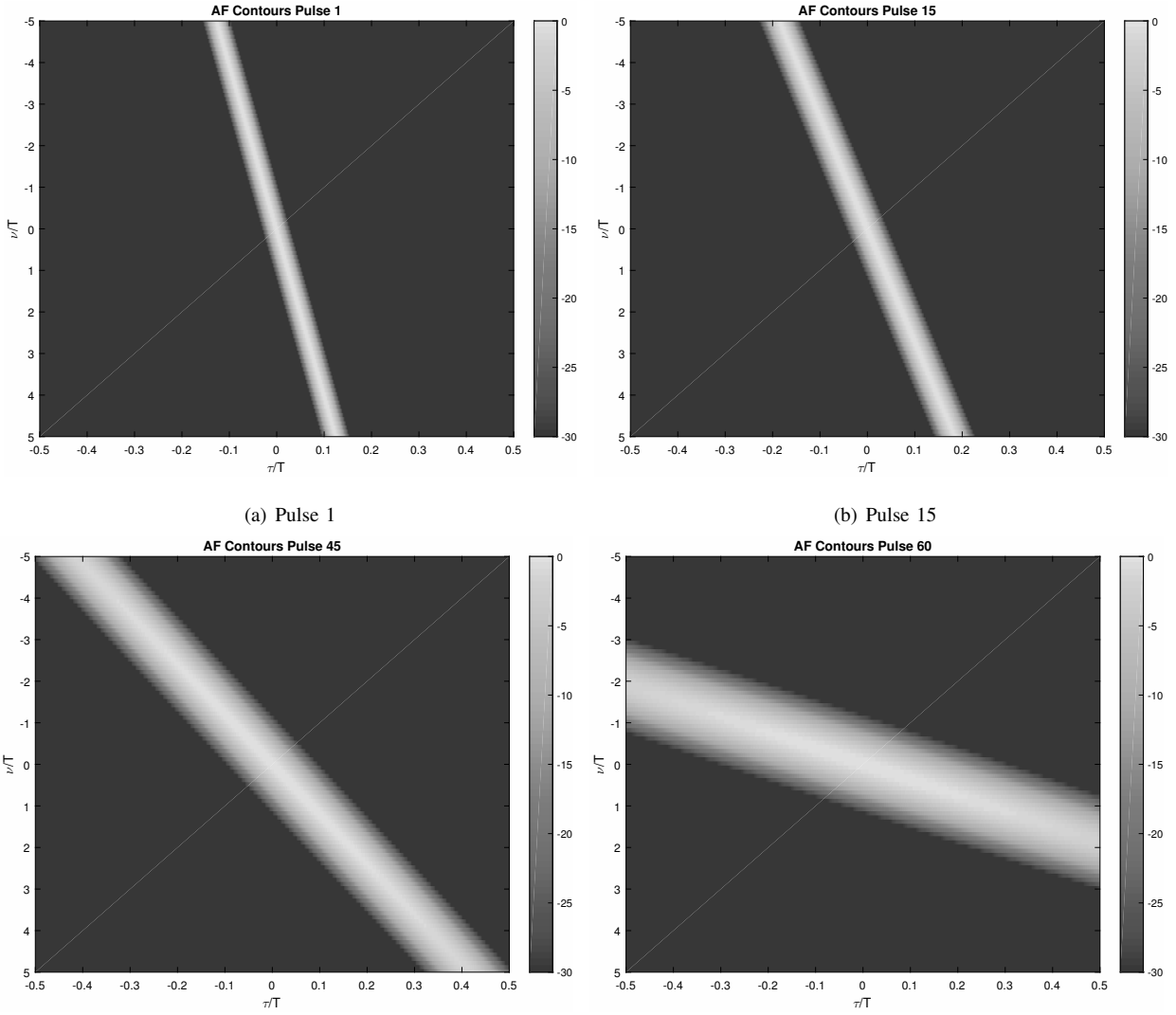

(a) Pulse 1

(b) Pulse 15

(c) Pulse 45

(d) Pulse 60

Fig. 3. Ambiguity Function (AF) for the case of $B_{min} = 5$ MHz. The plots are relative to one Monte Carlo realisation.

range-velocity diagram does not show significant difference with respect to the previous case of Figure 1. The results in Figure 7 show that the pulse duration is kept largely constant during the mission until it is reduced to avoid eclipsing. Interestingly, results show that the optimisation criterion that minimises the determinant of the matrix $\mathbf{S}$ converges to a solution consisting of frequency unmodulated pulses.

Figure 8 shows the range and radial velocity accuracy achieved at each pulse. As expected, because the pulse duration decreases and the SNR increases when the interceptor approaches the target the range accuracy also increases. The pulse duration for the case with $B_{min} = 5$ MHz reaches lower values than that relative to the case with no constrains in range resolution and this results in a better range accuracy (see element (1,1) of the matrix in Eq. 17). The radial velocity accuracy also decreases as the interceptor approaches the target but, overall, is very large. This is due to the short time observation interval, related to the exploitation of just one radiated pulse. This

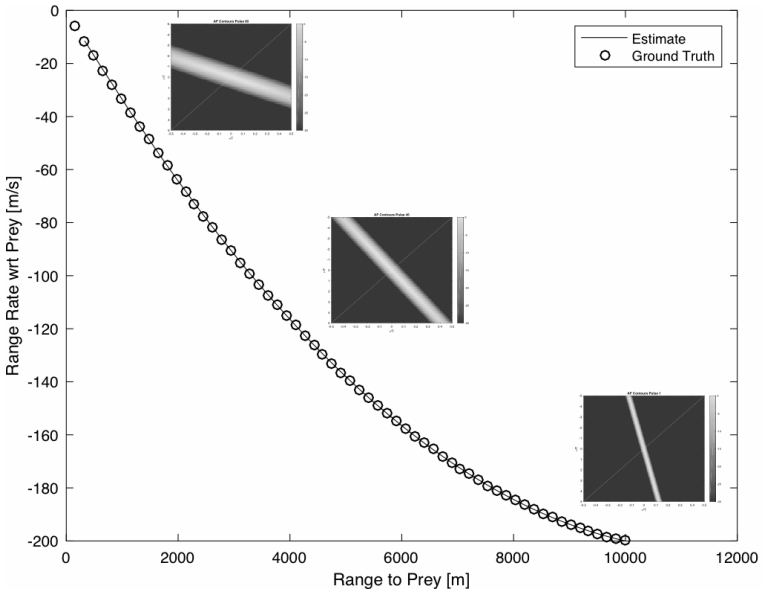

Fig. 4. Plots of the rotating AF superimposed to the range-velocity diagram. The figure shows the AF rotates anti-clockwise when the interceptor approaches the target. The plots are relative to one Monte Carlo realisation.

is in agreement with previous results (e.g. [12] and [13]). Results show that the Doppler accuracy reaches better values for the case with no constraints in range resolution and this is because, in this case, the algorithm converge to a frequency unmodulated waveform design (that is $b_G = 0$).

V. Conclusion

In this paper, we have presented an algorithm that allows an interceptor aircraft with an on-board radar to adapt its trajectory in order to intercept a target and automatically optimise the transmitted waveform on a pulse to pulse basis. To achieve this, we have suitably combined two techniques, namely the optimal Linear Quadratic Gaussian (LQG) control law and the fore-active control of the radiated waveform. The case study takes inspiration from existing predator-prey relationships in nature, such as that of a bat which captures a moth or a butterfly. The bat during its search, acquisition, tracking and interception of the insect adjusts both its trajectory to approach the prey and adaptively changes the radiated waveform of the echolocation calls in order to improve the localisation of the prey. Simulation results show that the interceptor can successfully reach the target within the predefined number of transmissions and automatically adapt the waveform during the mission. Future work will look at using different types of waveform designs and different optimisation criteria. The work will be extended to the the case of a train of pulses to take into account of a more realistic coherent integration time and a more realistic Doppler resolution. When a train of pulses is used, the FIM of the estimates of range and radial velocity presented in Eq. 17 is no longer valid. Using a train of pulses therefore requires the calculation of the FIM of the pulsed waveform and new calculations to obtain the expressions of the waveform parameters that minimise the determinant of the residual matrix. The case of the bat will be further studied by expanding the algorithm presented in this paper to the wideband case.

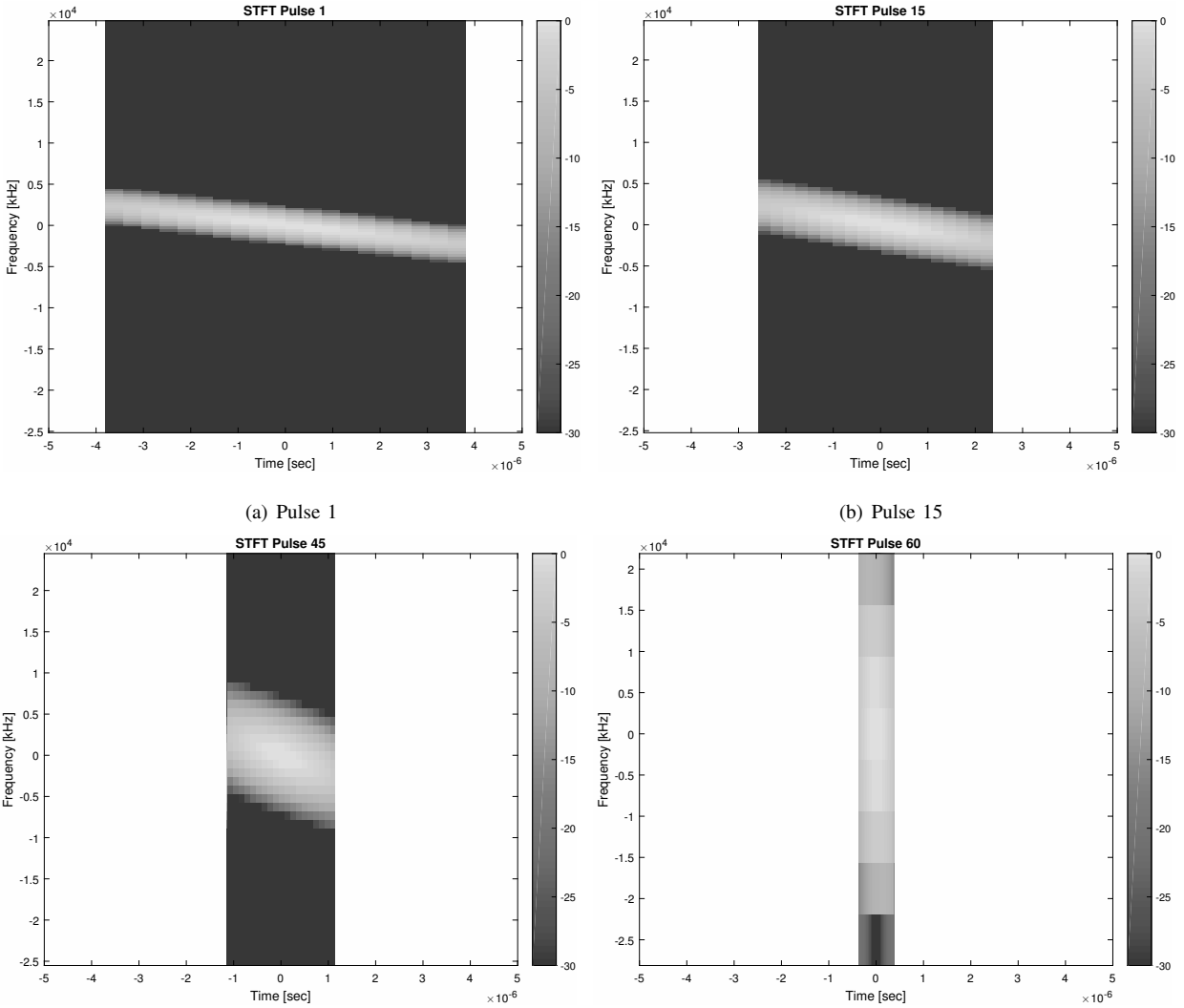

(a) Pulse 1

(b) Pulse 15

(c) Pulse 45

(d) Pulse 60

Fig. 5. Spectrograms for the case of $B_{min} = 5$ MHz. The plots are relative to one Monte Carlo realisation.

REFERENCES

[1] M. W. M. G. Dissanayake, P. Newman, S. Clark, H. F. Durrant-Whyte, and M. Csorba, "A solution to the simultaneous localization and map building (SLAM) problem," *IEEE Transactions on Robotics and Automation*, vol. 17, no. 3, pp. 229–241, Jun 2001.

[2] M. Athans, "On optimal allocation and guidance laws for linear lnterception and rendezvous problems," *IEEE Transactions on Aerospace and Electronic Systems*, vol. AES-7, no. 5, pp. 843–853, Sept 1971.

[3] D. Kershaw and R. Evans, "Optimal waveform selection for tracking systems," *IEEE Transactions on Information Theory*, vol. 40, no. 5, pp. 1536–1550, Sep 1994.

[4] C. Baker, H. Griffiths, and A. Balleri, "Biologically inspired waveform diversity (in Waveform Design and Diversity for Advanced Radar Systems)," *Institution of Engineering and Technology, Series on Radar, Sonar, Navigation and Avionics*, pp. 149–172, 2012.

[5] P. Flandrin, *Animal Sonar: Processes and Performance*. Boston, MA: Springer US, 1988, ch. Time-Frequency Processing of Bat Sonar Signals, pp. 797–802.

[6] F. Hlawatsch and G. F. Boudreaux-Bartels, "Linear and quadratic time-frequency signal representations," *IEEE Signal Processing Magazine*, vol. 9, no. 2, pp. 21–67, April 1992.

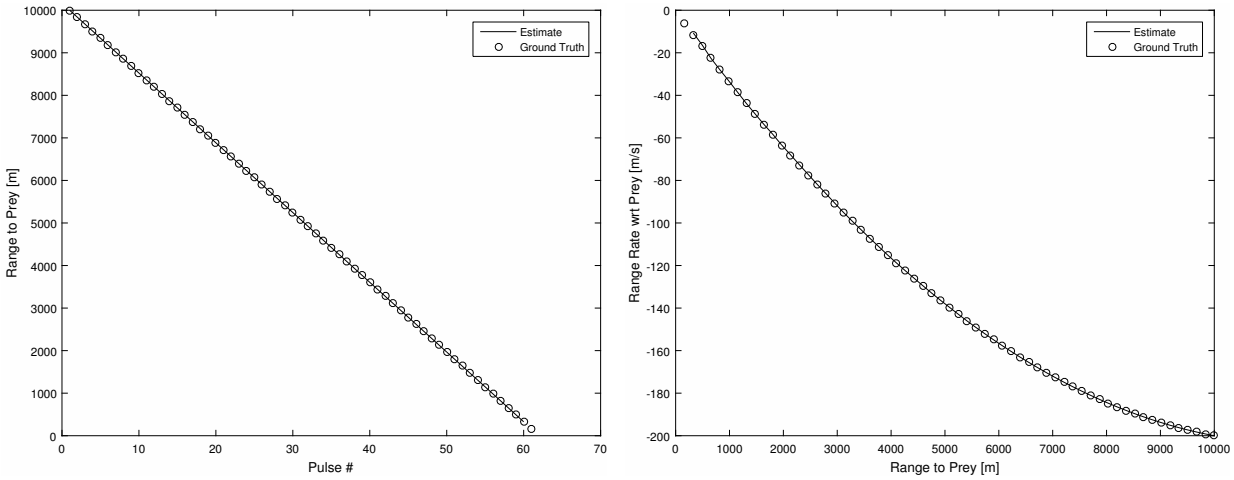

(a) Range vs Pulse (b) Range vs Range-rate

Fig. 6. a) Distance between the interceptor and the target at each transmission and b) Plot of the estimated range and velocity with respect to the ground truth at each transmission. The plots are relative to one Monte Carlo realisation.

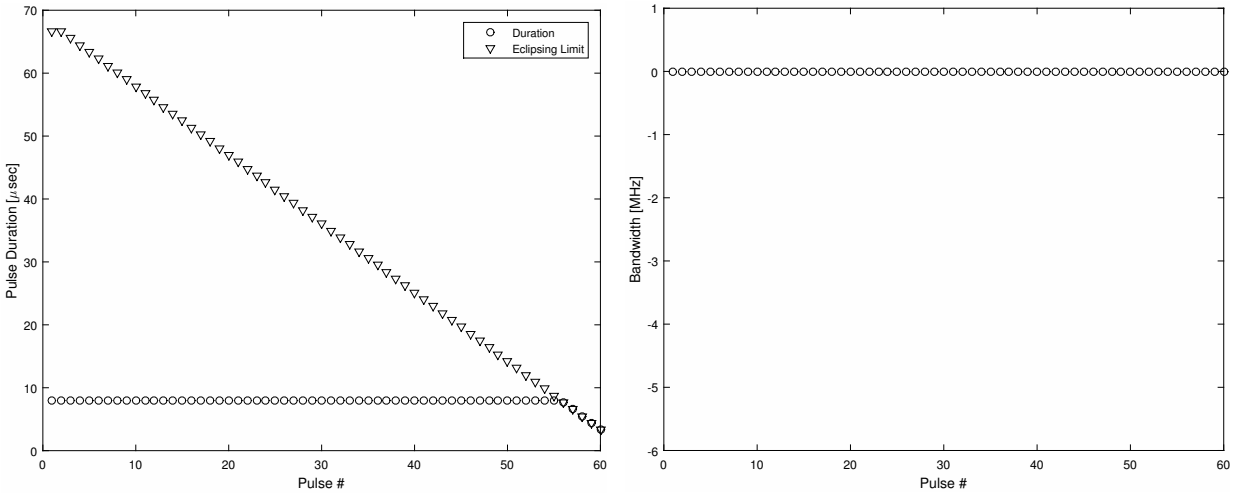

(a) Pulse Duration (b) Bandwidth

Fig. 7. a) Duration and b) bandwidth of the chirp with Gaussian envelope as a function of the transmitted pulse number when no constraints on the bandwidth are applied. The plots are relative to one Monte Carlo realisation.

[7] P. J. Nahin, *Chases and escapes: the mathematics of pursuit and evasion*. Princeton University Press, 2012.

[8] A. Farina, "Cognitive Radar Signal Processing," *Key Note Speech, IET International Radar Conference, Hangzhou, China*, 14-16 Oct. 2015.

[9] H. L. Van Trees, *Detection, estimation and modulation theory, Part III. Radar-Sonar signal processing and Gaussian signals in noise.* Wiley, 2001.

[10] C. E. Cook and M. Bernfeld, *Radar Signals:an introduction to theory and application.* Artech House, 1987.

[11] E. Kelly, "The radar measurement of range, velocity and acceleration," *IRE Transactions on Military Electronics*, vol. MIL-5, no. 2, pp. 51–57, April 1961.

[12] A. Dogandzic and A. Nehorai, "Cramer-Rao bounds for estimating range, velocity, and direction with an active array," *IEEE Transactions on Signal Processing*, vol. 49, no. 6, pp. 1122–1137, Jun 2001.

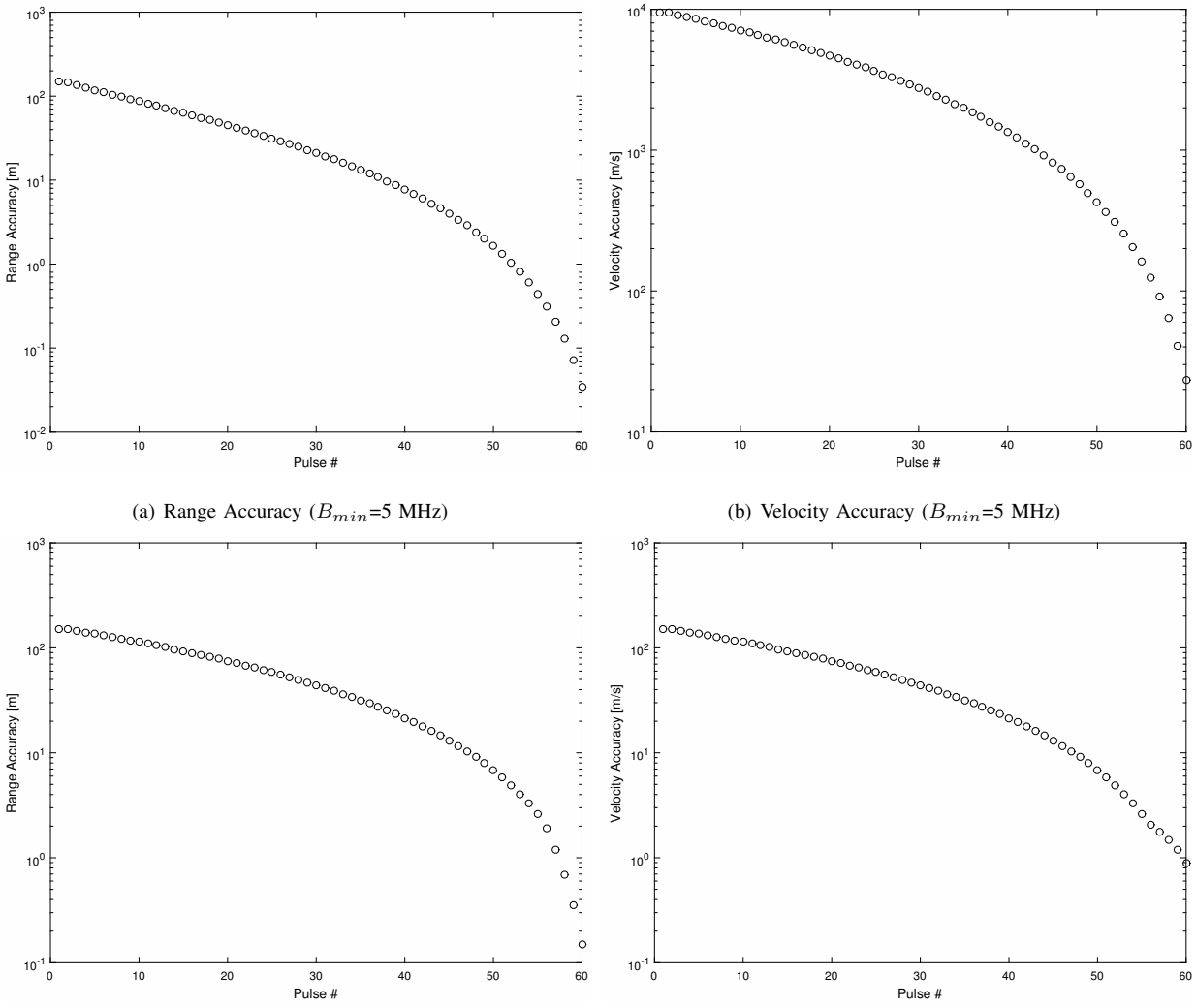

(a) Range Accuracy (B_{min}=5 MHz)

(b) Velocity Accuracy (B_{min}=5 MHz)

(c) Range Accuracy

(d) Velocity Accuracy

Fig. 8. a) Range and b) velocity accuracy of the chirp with Gaussian envelope as a function of the transmitted pulse number when a constraint on the bandwidth is applied. c) Range and d) velocity accuracy when no constraints on the bandwidth are applied The plots are relative to one Monte Carlo realisation.

[13] A. Balleri and A. Farina, "Ambiguity function and accuracy of the hyperbolic chirp: comparison with the linear chirp," *IET Radar, Sonar and Navigation*, Online May 2016.

[14] R. A. Singer, "Estimating optimal tracking filter performance for manned maneuvering targets," *IEEE Transactions on Aerospace and Electronic Systems*, vol. AES-6, no. 4, pp. 473–483, July 1970.